Single molecules in soft matter : a study of biomolecular conformation, heterogeneity and plasmon enhanced fluorescence

Yuan, H.

Cover Page

Universiteit Leiden

Leiden University
Repository

The handle http://hdl.handle.net/1887/22072 holds various files of this Leiden University dissertation.

Author: Yuan, Haifeng
Title: Single molecules in soft matter : a study of biomolecular conformation, heterogeneity and plasmon enhanced fluorescence
Issue Date: 2013-10-29

3 Temperature-cycle microscopy reveals single-molecule structural heterogeneity

Abstract – Our previous temperature-cycle study reported FRET transitions between different FRET states on FRET labeled polyprolines. The conformational origin of such transition, however, was difficult to determine. In this work, we apply temperature-cycle microscopy on single FRET labeled polyproline and dsDNA molecules and compare their responses to resolve the conformational origin of different FRET states. We observe different steady-state FRET distributions and different temperature-cycle response in the two samples. Our temperature-cycle results on single molecules resemble the results in steady-state measurements but reveal a dark state which could not be observed otherwise. By comparing the timescales and probabilities of different FRET states in temperature-cycle traces, we assign the structural heterogeneity reflected by different FRET states to linker dynamics and dye-dye separations. The dark state and low-FRET state are likely due to dye-dye interactions at short separations.

3.1 Introduction

Fluorescence resonance energy transfer (FRET) between FRET labels, which consist of one donor and one acceptor, proceeds via a dipole-dipole interaction. Thus, it is sensitive to the distances of 2-10 nm between FRET labels and often referred to as a "spectroscopic ruler" [37, 86]. Changes on FRET efficiency reflect conformational changes or interactions [44, 47, 107]. Suppressing ensemble averaging, single-molecule FRET has been broadly applied for probing molecular conformational changes and interactions in past decades [3, 12, 43, 82, 108–112]. FRET efficiency (E), which describes the fraction of energy transferred from donor to acceptor, can be calculated from the donor's intrinsic fluorescence lifetime (τ_{D0}) and that in presence of the acceptor (τ_{DA}), $E = 1 - \tau_{DA}/\tau_{D0}$. [37] Alternatively, FRET efficiency can also be calculated from the number of detected photons at donor (n_D) and acceptor (n_A) wavelengths, $E = n_A/(n_D + n_A)$ [12]. In either way, it requires at least several dozens of photons to determine FRET efficiency. Hence, the time resolution of single-molecule FRET is determined by photon statistics. Due to the limited emission rate of individual fluorophores and the limited instrumental detection efficiency, the time resolution is limited to a few milliseconds. Many biological process, however, take place on a time scale faster than milliseconds [85, 113]. To access fast dynamics of single molecules in real time, one has to increase the emission rate of fluorophores. By directly applying very intense laser excitation [41] or adding photoprotective agents [114], sub-milliseconds temporal resolution on single-molecule FRET has been demonstrated. Nevertheless, due to limited dwell time of the molecule in the observation volume, observing the same individual molecules for a long time without immobilizing them onto surfaces is still difficult.

To follow micro-second dynamics on a same molecule for long times without the complication of immobilization, a temperature-cycle technique was proposed [51]. This temperature-cycle method is closely related to the well established temperature-jump method at room temperature [52]. In temperature-cycle measurement, the extreme temperatures are chosen such that the dynamics of interest will be frozen at the low temperature and be activated at the high temperature. A dynamical process can thus be studied as a consecutive series of snapshots of frozen states with controllable time steps. In this method, the time resolution is limited only by the heating and cooling times, which are typically around 3-4 microseconds in the focal spot [51]. A schematic view of the temperature-cycle method is shown in figure 3.1. In previous work, we demonstrated temperature-cycle microscopy on FRET labeled all-trans polyprolines in glycerol [115]. All-trans polyproline possesses a helix structure

and is rather rigid. It was used as a model system to demonstrate FRET as a spectroscopic ruler [86]. Embedded in supercooled glycerol, FRET-labeled short polyproline constructs showed broad distributions in FRET values. Furthermore, we observed reversible transitions between a high FRET value and a low FRET value on individual FRET constructs by applying temperature cycles between $170\,\mathrm{K}$ and $250\,\mathrm{K}$ [115]. Such observations indicate conformational changes of the molecule. However, it is difficult to determine the origin of the FRET transitions.
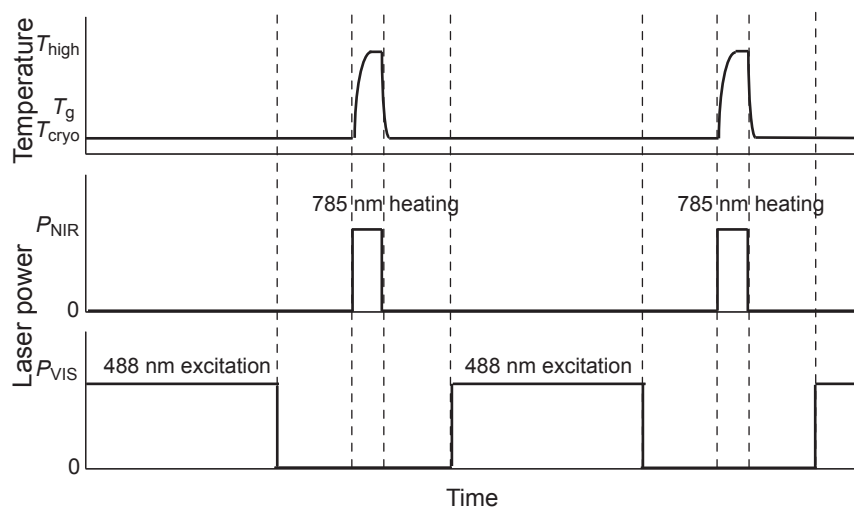
Figure 3.1: (a) Scheme of temperature-cycle method. The evolution of dynamics is allowed or frozen by fast temperature modulations by a NIR laser beam. While the molecule is frozen at low temperature of the cycle, another laser is used for probing states of the molecule optically. Alternatively applying sequences of laser beams, dynamics of the molecule can be recorded in series of snapshots.

Besides the dynamics of the polyproline chain itself [99, 100, 116], many other factors may influence the FRET distribution or timetrace, such as dye orientations, dynamics of linkers [100, 117–122] and dye photophysics [123–128]. Among the above mentioned factors, linker dynamics has received much attention since it can significantly influence FRET experiments. For instance, long and flexible linkers may bring FRET dye pairs close to each other and allow dye-dye interaction to take place [117, 124]. Di Fiori *et al.* found that dye-dye interactions at short separations lead to multiple-step fluorescence timetraces in single-molecule FRET measurements [124]. However, such interactions also depend on the dye pairs used in experiments [124]. Recent mole-

cular dynamics simulations by Hoefling *et al.* have shown that dynamics of the dye and the linker can induce extra structural heterogeneity and thus influence measured FRET [118]. The dye molecules with floppy and long linkers can get into contact with the polyproline chains due to hydrophobic interactions [118], thus quenching can take place [129].

In the hope of telling apart different factors which influence FRET, we adapt our temperature-cycle microscope to access dye orientations and fluorescence lifetimes by adding a polarization-dependent detection and a time-correlated single photon counting (TCSPC) system. To access photon information with additional dimensions, better photon statistics is required. In temperature-cycle measurements, one can simply extend the excitation duration in each period to collect as many photons as needed. However, this will reduce the number of temperature-cycle measurements on single molecules before photo-bleaching. Alternatively, we improve the collection efficiency of the optical system in our cryostat by introducing a hemispherical solid immersion lens (SIL). At room temperature, the numerical aperture (NA) of the optical system can be increased by liquid-immersion techniques. However, liquid immersion can hardly be applied for low-temperature microscopy due to phase transitions of liquids. Instead, we can use a hemispherical solid immersion lens (SIL). When the incident light is focused through the hemispherical solid immersion lens (n_{SIL}) at its center, the light wavefront will not be disturbed by the air-solid interface. In this way, the NA can be increased by a factor of n_{SIL} [130–135]. Being achromatic at its center, a SIL of hemispherical shape has been used to improve NA of optical systems in microscopy and spectroscopy applications [131, 136, 137]. In addition to a SIL, we use a single-component reflecting objective for following reasons. (i) Built on a single piece of fused silica, the single-component reflecting objective possesses superb stability at low temperatures [138, 139]. (ii) It is achromatic since it works with pure reflecting optics. (iii) It has a long working distance of more than 3 mm, thus we can use SILs with diameters of up to 3 mm. Although it has a small numerical aperture (NA, about 0.6), the total NA after adding a SIL of $n_{SIL} = 2$ can reach 1.2.

Here, we first characterize the hemispherical solid immersion lens and the single-component reflecting objective using fluorescent beads. We then apply this optical system for single-molecule temperature-cycle studies on both FRET-labeled polyproline and double-stranded DNA. Simultaneously measuring the fluorescence intensity and polarization while applying temperature cycles, we compare the results on FRET-labeled polyproline and double-stranded DNA.

3.2 Experimental
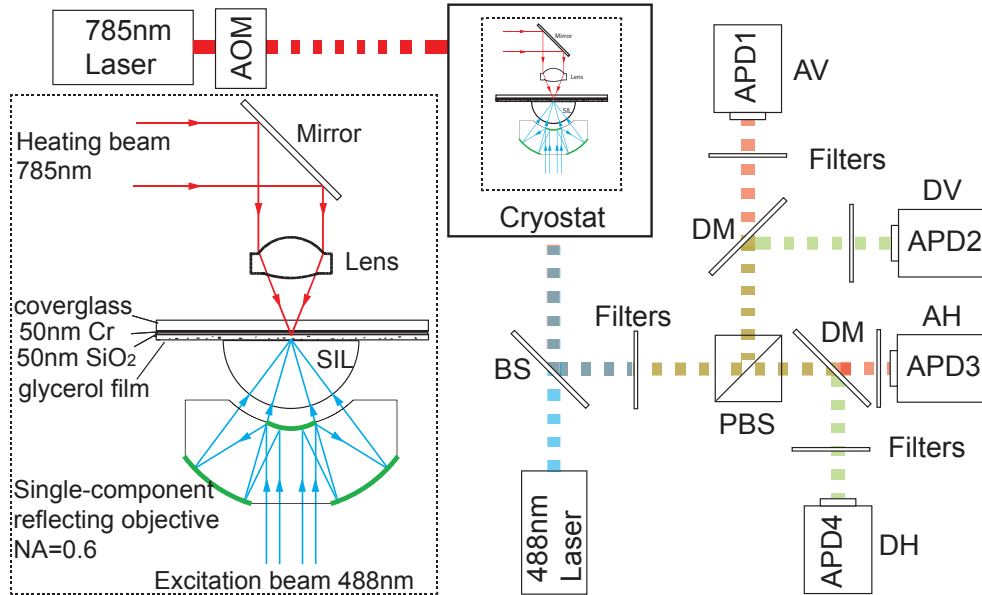
Figure 3.2: Scheme of experimental set-up. The optics inside the cryostat is enlarged and shown on the left. The heating laser is at 785 nm, while the excitation laser is at 488 nm. The two laser beams enter the cryostat through two optical windows. They are then focused and overlapped on the same position at the sample. After the fluorescence photons are collected by the objective, they are firstly separated into two more branches according to their polarization by a polarization beam splitter (PBS). Afterwards, each of the two paths is separated into two paths according to their wavelengths by dichroic mirrors (DM). After proper filters, they are detected by four APDs.

The home-built beam-scanning confocal microscope with a cryostat is described in detail in previous work by Zondervan *et al.* [51]. A scheme of the optical setup is shown in figure 3.2. A 785 nm continuous-wave (CW) diode laser (TOPTICA Photonics AG) modulated by an acousto-optic-modulator (AOM) is employed as the heating source. The heating beam is directed by a near-infrared (NIR) mirror and focused on the chromium film by an aspheric lens. The excitation beam from a pulsed 488 nm laser (BDL-488, Becker&Hickl GmbH) operating at 50 MHz is circularly polarized. After a pair of scanning mirrors and a telecentric system, it enters the cryostat from the bottom window. The excitation beam is then focused by the objective-SIL assembly on the

sample-SIL interface. The emitted photons are collected by the same objective and directed to the detection part by a beam splitter. After a 488 nm notch filter and a 774 nm shortpass filter, the fluorescence photons are separated by a polarization beam splitter into two paths according to their polarization. Before reaching the avalanche photodiodes (APDs), each of the two polarizations is again divided into two paths according to the wavelength by dichroic mirrors (DM585) and filters (535/50 bandpass filters for donor fluorescence, 630/92 bandpass filters for acceptor fluorescence). In total, the photons are detected in four channels: donor fluorescence of vertical polarization (DV), donor fluorescence of horizontal polarization (DH), acceptor fluorescence of vertical polarization (AV) and acceptor fluorescence of horizontal polarization (AH). The detected fluorescence photons are then recorded by a TCSPC system (TimeHarp200, PicoQuant).

3.2.1 Characterization of SIL

We first use fluorescent beads to characterize the optical system. A suspension of 20 nm fluorescent beads from stock was diluted with MilliQ water and mixed with glycerol in a 1:1 volume ratio. The glycerol suspension was then spin-coated at 6000 rpm for 60 seconds. It yielded a film of about 0.5-2 μm in thickness. A hemispherical SIL (LASF35 glass, n_{SIL}=2.02) of 2.5 mm diameter was then attached onto the glycerol film, as shown in figure 3.2. After the sample was inserted into the cryostat, it is dried by pumping vacuum and flushing dry helium gas for several times. Moreover, the sample was kept in an inert helium atmosphere throughout the entire experiment.

Two fluorescence images taken either with the reflecting objective or with the objective-SIL assembly under the same excitation power are shown in figure 3.3 (a) and (b). Imaging with the reflecting objective alone, the full-width at half-maximum (FWHM) of fluorescence beads is about 450 nm, as shown in figure 3.3 (a). The average fluorescence intensity is 46 photons per 10 ms. While imaging with the objective together with SIL, we observe an average FWHM of about 250 nm and an average fluorescence intensity of 140 photons per 10 ms. They are compared in figure 3.3 (c) and (d). The spatial resolution is improved by a factor of 1.8, which is very close to the value we would expect (n_{SIL}=2.02). The average intensity is improved by a factor of 3. This value, however, is somewhat lower than the expected value of 4.1 (n_{SIL}^2). It can be a consequence of two factors. Firstly, the high-refractive-index SIL is not anti-reflection coated, thus the reflection loss can be significant in both incident and collected light. Secondly, the distance between the fluorescent beads and the SIL-glycerol interface is not uniform. Thus, it can introduce variations on
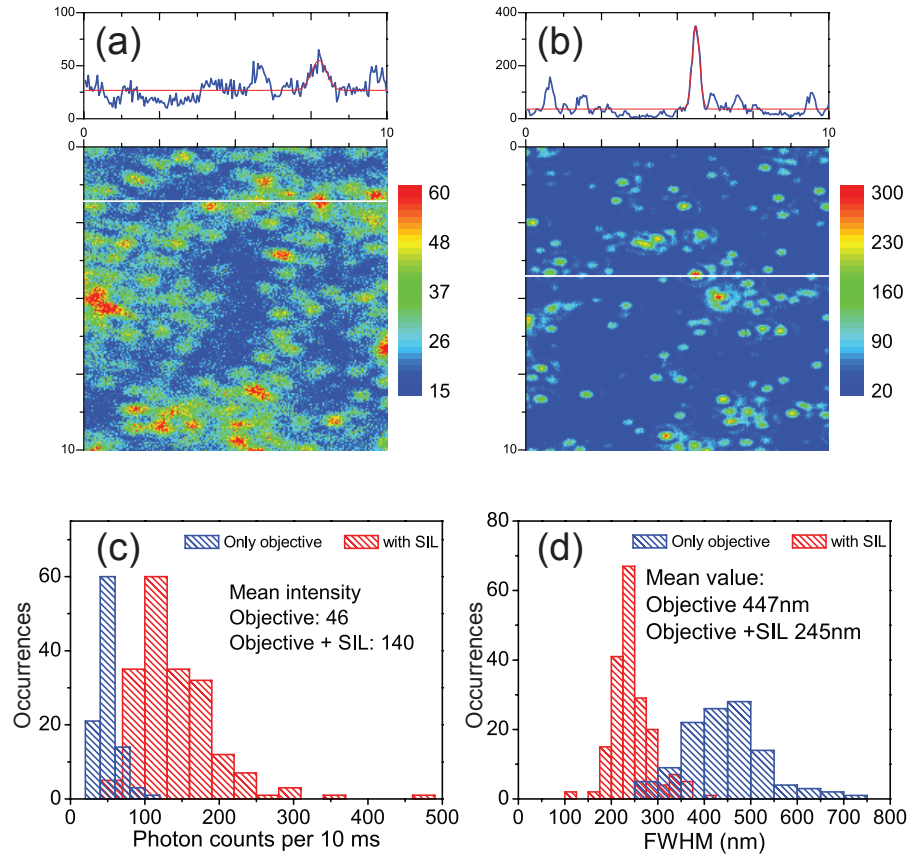
Figure 3.3: (a) A fluorescence image on a $10\,\mu$m $\times$ $10\,\mu$m area taken using the reflecting objective. (b) A fluorescence image on a $10\,\mu$m $\times$ $10\,\mu$m area taken using the reflecting objective in combination with a SIL. (c) Histograms of beads' fluorescence intensities measured by the reflecting objective with (red) and without the SIL (blue). The addition of a SIL improves the average intensity from 46 photons per $10\,$ms to 140 photons per $10\,$ms. (d) Histograms of FWHMs of fluorescence spots measured by the reflecting objective with (red) and without the SIL (blue). The use of a SIL improves the spatial resolution from $447\,$nm to $245\,$nm.

the collection efficiencies.
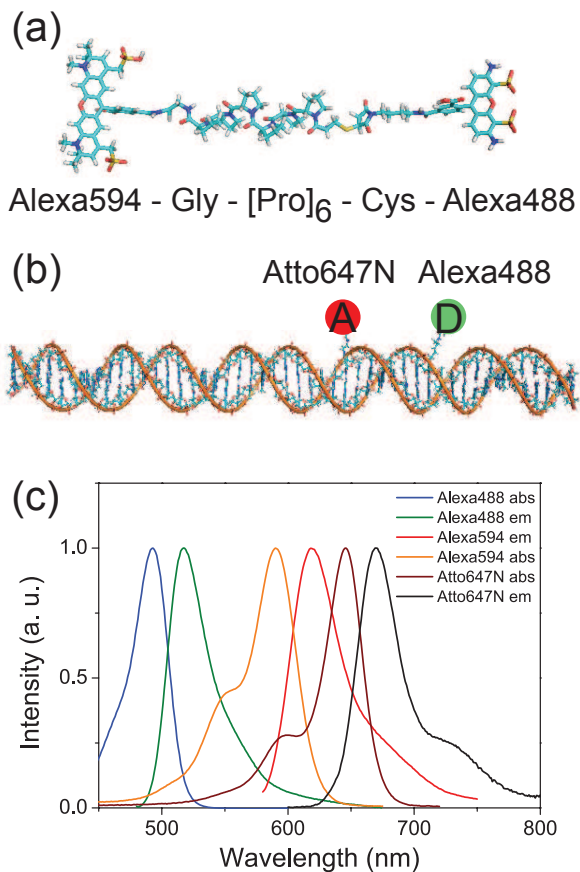
Figure 3.4: (a) Molecular structure of the FRET-labeled polyproline construct. (b) Molecular structure of dsDNA sample. (c) Alexa488, Alexa594, Atto647N absorption and emission spectra

3.2.2 Materials and methods

Glycerol was purchased from Sigma-Aldrich and used as received without further purification. Polyproline of 6 residues (Pro6) and 20 residues (Pro20) were labeled at two ends, as shown in figure 3.4 (a). Alexa488, the donor molecule, was attached to a cysteine residue at one end of the peptide chain. The acceptor, Alexa594, was attached to a glycine residue at the other end of the peptide chain. We estimate the end-to-end contour length of the peptide to be about 2.4 nm. Double-stranded DNA (dsDNA) molecules of 48 basepairs were labeled with Alexa488 and Atto647N on different strands, as shown in

figure 3.4 (b). The sequence of one chain is 5'-d(GGA CTA GTC TAG GCG AAC GTT TAA GGC GAT CTC TG**T**(Alexa488) TTA CAA CTC CGA)-3'. The sequence of the other chain is 5'-d(TCG GAG TTG TAA ACA GAG A**T**(Atto647N)C GCC TTA AAC GTT CGC CTA GAC TAG TCC)-3'. The bold letters show the position where the fluorophores are attached. The two fluorophores were separated by 7 basepairs, which corresponds to a distance of 2.5 nm. Absorption and emission spectra of both FRET pairs are shown in figure 3.4 (c).

Polyproline samples labeled with Alexa488 and Alexa594 were diluted to 10^{-12} M in 50 mM phosphate buffer solution, the pH was adjusted to 7.0. ds-DNA labeled with Alexa488 and Atto647N was diluted to 10^{-12} M in TRIS (tris(hydroxymethyl)aminomethane) buffer, which contains 20 mM TRIS, 100 mM NaCl and 10 mM MgCl$_2$. The pH was adjusted to 7.5. After diluting to desired concentrations in buffer solutions, the sample solutions were mixed with glycerol at a volume ratio of 1 : 1. The sample solutions were then spin-coated onto glass substrates coated with 50 nm Cr and 50 nm SiO$_2$. 60-second spin-coating at 6000 rpm resulted in a sample film of about 0.5-2 μm in thickness. After spin-coating, the SIL was attached onto the glycerol-water film. The sample was then mounted onto a three-dimensional piezo-stage and was inserted into the cryostat. Before cooling down, the samples inside the cryostat were dried by pumping and flushing with dry helium gas for several times. They were then kept in an inert and dry helium atmosphere throughout the entire experiment. The samples were cooled directly from room temperature (290 K) to 170 K at a cooling rate of 5 K per hour.

In steady-state measurements, the temperature was fixed at 170 K, which is already 20 K below the glass transition temperature of glycerol. At this temperature the FRET constructs' motions are frozen, thus they show almost constant FRET efficiency. The FRET efficiency (E) is calculated from fluorescence timetraces using the following equation:

$$E = \frac{n_{AH} + n_{AV}}{\gamma(n_{DH} + n_{DV}) + n_{AH} + n_{AV}} \tag{3.1}$$

where n_{AH}, n_{AV}, n_{DH} and n_{DV} are the detected fluorescence intensities from the corresponding APDs. $\gamma = \frac{\Phi_A \eta_A}{\Phi_D \eta_D}$ is the correction factor for differences in dye quantum yields (Φ_A, Φ_D) and collection efficiencies (η_A, η_D). In the current experimental set-up, γ=0.6 for Alexa488 and Alexa594 while γ=0.7 for Alexa488 and Atto647N. The crosstalk from donor channel to acceptor channel is less than 10%. Therefore, we only take the FRET values above 0.15 into account. The donor's fluorescence lifetime is measured by deconvoluting the instrumental response function (IRF) from the TCSPC histogram and mono-

exponential fitting. Linear dichroism (D) is calculated using the equation below:

$$D = \frac{n_H - n_V}{n_H + n_V} \tag{3.2}$$

where n_H is the fluorescence intensity at the horizontal polarization and n_V is the fluorescence intensity at the vertical polarization.

In temperature-cycle measurements, the same parameters were applied to both Pro6 and dsDNA samples. The cryostat temperature was kept at 170 K (± 0.1 K) throughout the entire experiment. The higher temperature of a temperature cycle was chosen to be 290 K. In each temperature cycle, the heating beam was applied for 20 μs and the 50 MHz-pulsed excitation beam was applied for 500 ms.

3.3 Results

The conformations of FRET constructs are frozen in glycerol at 170 K. Therefore, they show constant signals in both donor and acceptor fluorescence. A typical fluorescence timetrace of a Pro6 construct is shown in figure 3.5 (a). Although noisy, the fluorescence intensities in donor (light blue) and acceptor(red) channels are almost constant until a sudden drop in both intensities, which is the signature of a single construct. The single-step drop in fluorescence signals is most likely due to photobleaching of the donor fluorophore. Using average intensities at donor and acceptor channels, we estimate the FRET efficiency of this molecule to be 0.63. The donor fluorescence lifetime decay of the same molecule is shown in figure 3.5 (b). Fitting the lifetime decay with a mono-exponential function after deconvolution of the instrumental response function (IRF), yields a donor fluorescence lifetime of 2.1 ns.

Correlation between FRET efficiencies and donor fluorescence lifetime is shown in figure 3.5 (c) and (d). In figure 3.5 (c), each green spot represents a measurement on a single molecule. The horizontal position corresponds to its donor fluorescence lifetime and the vertical position corresponds to its FRET efficiency. The red line shows the expected correlation between FRET efficiency and donor fluorescence lifetimes, $E = 1 - \tau_{DA}/\tau_{D0}$ (τ_{D0}=3.5 ns, measured on Alexa488-labeled polyproline). The correlation observed in our measurements on 98 single Pro6 molecules is weak and shows deviations from theory for molecules with high FRET efficiencies. That is probably due to their low donor fluorescence intensities. For this reason, the donor fluorescence lifetimes of molecules with FRET efficiencies above 0.9 are not shown in figure 3.5 (c). Similar measurements on Pro20, which has a longer interdye distance,
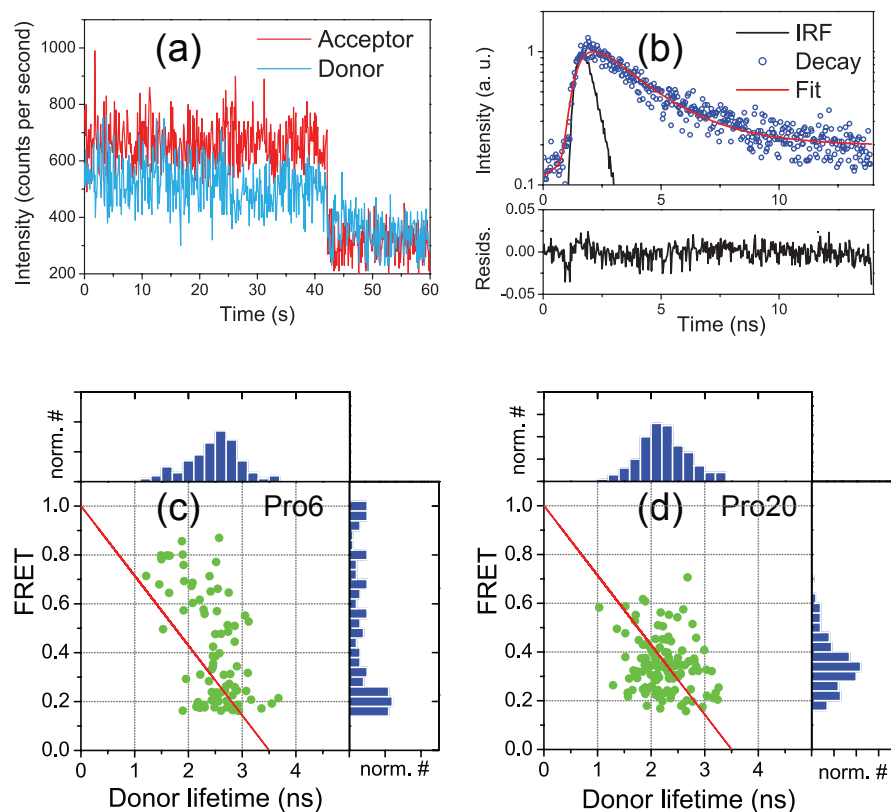
Figure 3.5: (a) Typical steady-state fluorescence timetraces recorded at 170 K on a single FRET construct (Pro6) under 50 MHz pulsed excitation. Both the donor (light blue) and the acceptor (red) show almost constant fluorescence intensities before bleaching. It yields a FRET efficiency of 0.63.(b) The donor fluorescence lifetime decay (blue circles) of the fluorescence trace in (a) and its mono-exponential fit (red) after deconvoluting IRF (black). The donor showed a fluorescence lifetime of 2.1 ns. (c) Correlation between donor fluorescence lifetimes and FRET efficiencies measured on single Pro6 molecules. (d) Correlation between donor fluorescence lifetimes and FRET efficiencies measured on single Pro20 molecules.

shows less deviations and hardly any correlation in figure 3.5 (d). Because of the low signal-to-background ratio, the lifetime measurements have a relative large error bar and thus provide little information.

Although the distances between the labeling positions of donor and ac-
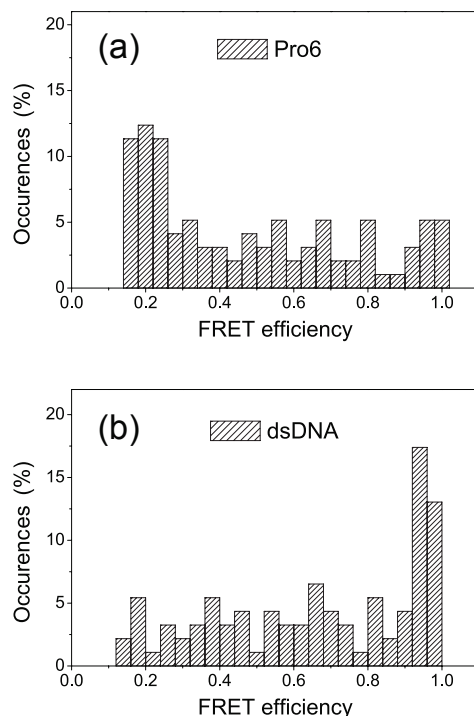
Figure 3.6: (a) Steady-state FRET histogram of Pro6. (b) Steady-state FRET histogram of dsDNA.

ceptor, 2.4 nm for the Pro6 sample and 2.5 nm for the dsDNA sample, are very similar, we observed surprisingly different FRET efficiency distributions at steady state (T=170 K). On the Pro6 sample, a broad FRET efficiency distribution with a significant low-FRET population was found, as shown in figure 3.6 (a). This observation is consistent with our previous experiments [115]. On the contrary, the dsDNA sample shows a large population at almost unity values, as shown in figure 3.6 (b). Despite some population at low-FRET values, the distribution agrees qualitatively with that Förster theory predicts for short interdye distances [37, 115].

Temperature cycles between 170 K and 290 K were applied on both Pro6 and dsDNA samples. Three reconstructed temperature-cycle traces are shown in figure 3.7. In figure 3.7 (a), a Pro6 molecule experienced more than 700 temperature cycles before bleaching. It showed dozens of transitions among three different FRET states: a dark state (D), a low-FRET state (L) and
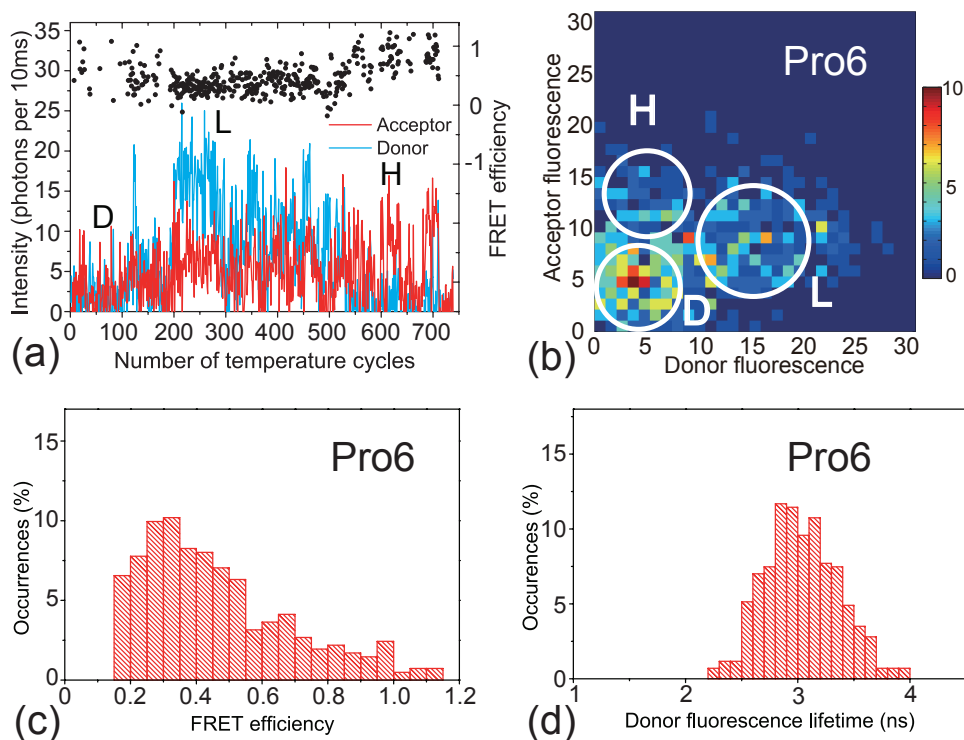
Figure 3.7: (a) A reconstructed temperature-cycle timetrace of donor (light blue) and acceptor (red) fluorescence on a single Pro6 molecule. (b) The correlation map of the donor fluorescence intensities against the acceptor fluorescence intensities of the trace shown in (a). The high-FRET state (H), the low-FRET state (L) and the dark state (D) are highlighted in white cycles. (c) The FRET efficiency histogram of the trace in (a). (d) The donor fluorescence lifetime histogram measured in each temperature cycle of the trace in (a).

a high-FRET state(H). We can recognize these three FRET states from the correlation histogram in figure 3.7 (b). In the dark state, both the donor and the acceptor remain dark in fluorescence. The low-FRET state shows high intensities in donor's fluorescence (light blue) and low intensities in acceptor's fluorescence (red). At the opposite, the high-FRET state shows a low donor fluorescence intensity but a high acceptor fluorescence intensity. The observed three states are different from previous reports of two FRET states (low-FRET and high-FRET) on Pro6 constructs. This may be due to the different temperature-cycle parameters applied during measurements [115]. In this work, we applied temperature cycles to higher temperatures (290 K instead

of $250\,\mathrm{K}$) with longer heating durations ($20\,\mu\mathrm{s}$ instead of $10\,\mu\mathrm{s}$). This allows the molecule's conformation to evolve for longer times at higher temperature. Thus, the transition to a dark state may not have been revealed in that previous study. Moreover, the dark state will not be reflected in the steady-state FRET histogram. The FRET histogram of the trace in figure 3.7 (a) is shown in figure 3.7 (c). It shows a broad distribution and a major population in low-FRET values. Besides FRET efficiencies, the donor fluorescence lifetime is also measured for each temperature cycle. The histogram is shown in figure 3.7 (d). Both the FRET efficiencies and the donor fluorescence lifetimes closely resemble Pro6's steady-state distributions shown in figure 3.5 (c).

Under the same temperature cycles, a dsDNA molecule showed reversible transitions between a low-FRET state and a high-FRET state during 3200 temperature cycles without the presence of any dark state, as shown in figure 3.8 (a). Intensities of donor and acceptor fluorescence showed anticorrelated changes in the timetraces. Acceptor fluorescence intensity occasionally dropped to background level while donor fluorescence increased to about 15 photons per $10\,\mathrm{ms}$. After more than 10 times fast switching between the low-FRET and high-FRET states, the acceptor bleached. We also observed a recovery in donor's fluorescence right after the acceptor bleached. The donor finally bleached after a few dozens more temperature-cycles. However, another dsDNA molecule showed a different behavior, as shown in figure 3.8 (b). During the 2500 temperature-cycles, this dsDNA molecule showed high intensities in acceptor fluorescence before it bleached. Instead of switching between low-FRET and high-FRET states, it showed several different intensity levels in the acceptor fluorescence timetrace. Meanwhile, it showed very low intensities in donor fluorescence without much fluctuation. In the beginning 1500 temperature cycles, the acceptor fluorescence was about 23 photons per $10\,\mathrm{ms}$. It then decreased to around 20 photons per $10\,\mathrm{ms}$ and lasted for about 800 temperature-cycles before further decreasing to 10 photons per $10\,\mathrm{ms}$. Shortly, it recovered to 20 photons per $10\,\mathrm{ms}$ and bleached. After the acceptor bleached, there was no recovery in donor fluorescence.

The FRET trace of the switching dsDNA molecule is shown in figure 3.8 (c). We can clearly see the two distinct FRET states. One displays high FRET values around 0.8. The other one shows low FRET values around 0.2. As we can see, the high-FRET state occupies most of the trace while the low-FRET state is rare and short-lived. This can also be reflected in the FRET histogram shown in figure 3.8 (d).

Besides FRET efficiencies, orientations of dyes were monitored by their fluorescence linear dichroism. However, in the temperature-cycle measure-
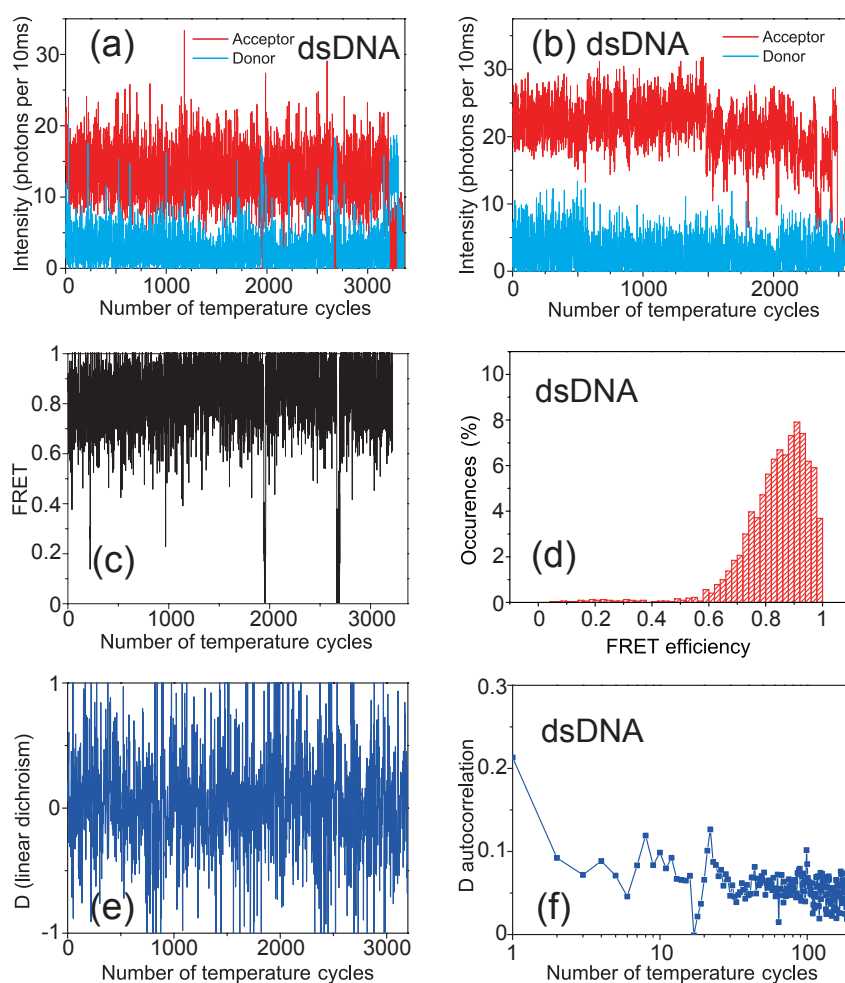
Figure 3.8: (a) A reconstructed temperature-cycle timetrace of donor (light blue) and acceptor (red) fluorescence on a single dsDNA molecule. (b) Another temperature-cycle timetrace on a single dsDNA molecule. (c) The calculated FRET efficiency trace of the fluorescence traces in (a). (d) The FRET histogram of the traces in (a). (e) The linear dichroism trace of the acceptor in (a). (f) The autocorrelation of the linear dichroism trace in (e).

ments on Pro6 and dsDNA, either the donor or the acceptor showed high fluorescence intensities alternatively. Thus, it is difficulty to follow the orientations of both dyes. Nevertheless, we observed reorientation of the strongly emitting one among the two dyes. Figure 3.8 (e) shows the linear dichroism

trace of the acceptor dye in the dsDNA molecule in figure 3.8 (a). The noisy trace shows fluctuations in linear dichroism, indicating changes in the acceptor's in-plane orientation. It does not show any obvious correlation to the measured FRET efficiencies. To characterize the rotational dynamics, the autocorrelation of the linear dichroism trace is calculated and is shown in figure 3.8 (f). It shows an almost flat correlation curve, thus fails to report the characteristic time of rotational dynamics. One possible reason is that the temperature-cycle parameters applied here are not optimal for probing rotational dynamics. The other possible reason is the low signal-to-noise ratio of our fluorescence traces.

3.4 Discussion

We have shown single-molecule FRET measurements on polyproline and ds-DNA molecules both in steady-state and under temperature cycles. In the following, we first discuss different results in steady-state measurements. Embedded in glassy glycerol, the guest molecules' conformations are frozen. Thus, their structural heterogeneity can be conserved and be reflected by FRET measurements. Broad FRET distributions were found in both Pro6 and dsDNA molecules. However, Pro6 molecules showed a major population in low FRET values while dsDNA molecules showed mainly high FRET values. Several possible factors may lead to such different results: (i) differences in chain dynamics of polyproline and dsDNA; (ii) different acceptors used for FRET; (iii) differences in volumes accessible to the dyes. Let us discuss them one by one in the following.

First of all, we comment on the differences in chain dynamics. All-trans polyproline is known to possess a helix structure and is rather rigid [86]. Its persistence length is reported to be longer than 5 nm [100]. Although cis-trans transitions can take place in proline residues and change the conformation of the polyproline chain, it is a rare process [118]. The double-helix chain of dsDNA is even more rigid than polyproline chains. It has a stable structure and its persistence length is 50 nm. Both Pro6 and dsDNA used in this work are shorter than their persistence lengths. Hence, we can consider both of them as rigid rods.

We then comment on the different acceptors. Though Pro6 and dsDNA are labeled with different acceptors (Alexa594 and Atto647N), their labeling positions are equally separated from that of the donor. In Pro6 molecules, donor and acceptor dyes are labeled at two ends of the peptide chain of 8 residues. The end-to-end contour length is about 2.4 nm. Instead of labeling

at two ends, dyes are labeled in the middle of the dsDNA chain but with a similar separation of 7 basepairs, which corresponds to about 2.5 nm. Both distances between labeling positions are much shorter than the Förster radii of FRET-pairs (about 5 nm). Hence, we would expect the major population to be at high FRET values for both samples.

The last but most likely reason for the different FRET distributions found on Pro6 and dsDNA is the difference in the accessible volumes for dyes. As mentioned, dyes are attached at two ends of the polyproline chain but in middle of the dsDNA chain. Thus, dyes in different samples can access different volumes as already demonstrated in several simulations and experiments [117, 118]. Attached at the ends of the peptide chain, the dyes in Pro6 can fully explore the volume around it, within the length of the linker [118]. Limited by both the linkers and double-helix around them, dyes attached on dsDNA have limited access to surroundings [117]. When the dyes are labeled at short separations, they could possibly come very close to each other (even into contact) to allow dye-dye interaction to take place [118, 124, 129]. In the molecular dynamics simulation on Alexa488 and Alexa594 labeled polyproline by Hoefling *et al.*, they found that the dye with the long and flexible linker can bend in and stick onto the polyproline chain for a long time due to hydrophobic interactions. The presence of such conformations can easily influence the observed FRET distribution of Pro6 by introducing extra interactions (either between dyes and polyproline chain or between dyes) which are not described by Förster theory. In dsDNA, similar dye-dye interaction can also occur [124]. But it happens less frequently, probably due to extra limitations on dye accessible volumes by DNA structures and less hydrophobic interaction. Furthermore, variations on measured FRET due to such conformational states strongly depend on the interdye distances. The dye-dye interaction will be less likely to happen if the interdye distance is longer. This is evident from the FRET distribution observed on Pro20, which has a longer interdye distance (about 7 nm). Pro20 showed a steady-state FRET distribution which is in fairly good agreement with that predicted by Förster theory.

In our temperature-cycle measurements on Pro6, three fluorescence states including a dark state, a low-FRET state and a high-FRET state were revealed. On dsDNA, a low-FRET state and a high-FRET state were found by applying temperature cycles. In the steady-state measurements, we can readily recognize the low-FRET state and the high-FRET state from FRET histograms of both samples (figure 3.6 a and b). However, the temperature-cycle measurements revealed a third state in which both donor and acceptor are dark in fluorescence on Pro6. This dark state, otherwise, can never be

revealed in steady-state measurements. Moreover, we observed multiple-level intensities in the acceptor fluorescence in the high-FRET state of dsDNA. The transitions between different FRET states implies conformational changes.

Different from real-time measurements, the dynamical process is recorded with snapshots of controlled step sizes in temperature-cycle measurements. We first comment on the time step of each temperature-cycle snapshot. In each temperature cycle, the molecule under investigation was brought to $290\,\mathrm{K}$ by a $20\,\mu\mathrm{s}$ heating pulse. Considering the time taken to reach the aimed temperature ($4\,\mu\mathrm{s}$ [51]), the molecule's dynamics evolves for $16\,\mu\mathrm{s}$ before being again frozen. Taking into account glycerol's different viscosity [93] from that of water, it corresponds to about $10\,\mathrm{ns}$ in water at the same temperature.

We now comment on the dyes' rotational dynamics. In dsDNA samples, reorientation of the acceptor can be recognized from the linear dichroism traces in figure 3.8 (e). However, autocorrelation of linear dichroism cannot report on the timescale of dye rotational time. This is probably because the temperature-cycle parameters were not optimized for such purpose. Rotational times of dyes labeled to dsDNA have been reported to be less than $1\,\mathrm{ns}$ in water solution at room temperature [117]. Therefore, the temperature cycles of $10\,\mathrm{ns}$ equivalent time step can hardly resolve the rotational dynamics that happens in less than $1\,\mathrm{ns}$.

Rotational dynamics of both dyes may influence FRET efficiencies because FRET proceeds via dipole-dipole interaction that depends on distance between two dipoles as well as the relative orientation of the dipoles [37]. Assuming both dyes to orient randomly [37, 83, 84], the FRET distributions for fixed interdye distances of $3\,\mathrm{nm}$ and $4\,\mathrm{nm}$ are shown in figure 3.9. At short interdye distances, we expected to observed mainly almost unity FRET values. Therefore, the probability to observe FRET changes induced by dyes' rotational dynamics will be very low in our Pro6 and dsDNA samples. It also explains why we did not observe any correlation between dye reorientation and measured FRET on dsDNA molecules. Thus, the FRET transitions observed upon temperature cycles are unlikely to be due to rotational motions of dyes.

To address dynamical origins of observed different FRET states on Pro6 and dsDNA molecules, we compare their timescales in the following. In Pro6, the dark state appeared frequently and occupied almost half the time of the trace. Moreover, the transitions from the dark-state to both high-FRET and low-FRET states were also observed frequently. Dozens of transitions between the three states took place in 700 temperature-cycles of $20\,\mu\mathrm{s}$. Furthermore, each state occupied at least several dozens (10-100) snapshots before a transition to different states occurred. This clearly indicate that the conformational
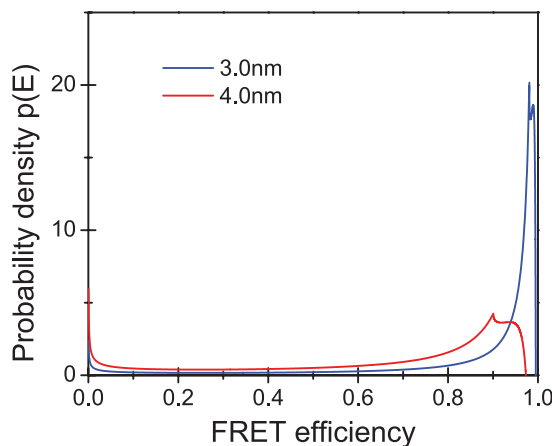
Figure 3.9: Calculated FRET probability density on 3 nm (blue) and 4 nm (red) interdye distances, assuming random orientation of both donor and acceptor dyes.

heterogeneity which induces such transitions happens on a relatively slow timescale. We speculate that slow dynamics correspond to sub-microsecond timescales in water solution. On the contrary, dsDNA molecules were in the high-FRET state for most of the time and showed only occasional transitions to the low-FRET state for short times. During 3200 temperature-cycles of $20\,\mu$s, less than ten transitions between high-FRET and low-FRET states took place. We also noted the low-FRET state in dsDNA was rare and short-lived (less than 50 temperature-cycles of $20\,\mu$s). These observations indicate that such transitions between different FRET states happen on a similar timescale but at a much lower probability in dsDNA.

The difference in timescales of the dark state and low-FRET state between Pro6 and dsDNA is most likely due to the interactions between linkers and chains, as suggested by molecular dynamics simulations. The long and flexible linker can bend in and attach onto polyproline and such process is a slow process compared to rotational motions of dyes [118]. Such conformations can indeed increase the chance to have the donor very close to the acceptor and interact.

We therefore attribute the dark state and the low-FRET state to the donor and the acceptor that are close to contact. When the two dyes are separated by distances on the order of van der Waals radii, their photophysical properties may alter reversibly with new non-radiative relaxation pathways offered by

electronic interactions [129]. Probably accompanying charge transfer at short distances, one of the dyes can enter a dark state. When this happens to the donor, both the donor and the acceptor will become dark in fluorescence, thus a dark period is observed. On the contrary, if this happens to the acceptor, we will only observe the fluorescence from the donor, thus a low-FRET state. The strength of such interactions depends on the separation between the donor and the acceptor. In Pro6 constructs, the donor and the acceptor have more chance to get close to each other due to sticking of the donor onto the polyproline chain and less limitation on accessible dye positions. On the contrary, the dyes in dsDNA constructs have less chance to interact with each other due to extra limitation on dye positions by DNA structures. Therefore, the dark state and the low-FRET state appears more frequently and lasts for longer times in Pro6 constructs but not in dsDNA constructs.

Therefore, we assign the different observations on Pro6 and dsDNA molecules under temperature cycles to the different accessible volumes for dyes. The multiple FRET states or intensity levels result from the dye-dye interactions at short interdye separations. The temperature-cycle results are in very good agreement with steady-state results and provide more insight into dynamics of these constructs.

3.5 Conclusion

We demonstrate both steady-state and temperature-cycle experiments on Pro6 and dsDNA samples. By applying temperature cycles, we reveal that complex dynamical processes occurred in molecules which were used as models to demonstrate FRET as a "molecular ruler". The multiple FRET states and dynamical transitions between these states show different behaviors in Pro6 and dsDNA samples. Comparing the timescales and probabilities of all these different FRET states, we assign them to structural heterogeneity that is related to linker dynamics and dye-dye separations. We attribute the multiple FRET states and multi-level intensities to dye-dye interactions at short interdye distances. We have demonstrated the temperature-cycle method as a powerful tool to study heterogeneous dynamics on a single-molecule scale using FRET. We found dsDNA molecules to better reveal FRET phenomena due to much reduced interaction between dye-linker and DNA chain. It would be interesting to further study two-level dynamical systems such as DNA hairpins [140–142] and Holliday-junctions [3, 44] using the temperature-cycle method in future work.

Acknowledgements